Naval Research Laboratory

Washington, DC 20375-5000

NRL Memorandum Report 6366

Near Field Turbulent Wake Predictions

M. B. STEWART

Laboratory for Computational Physics and Fluid Dynamics

November 8, 1988

SECURITY CLASSIFICATION OF THIS PAGE

REPORT DOCUMENTATION PAGE

1a. REPORT SECURITY CLASSIFICATION UNCLASSIFIED	1b. RESTRICTIVE MARKINGS
2a. SECURITY CLASSIFICATION AUTHORITY	3 DISTRIBUTION / AVAILABILITY OF REPORT Approved for public release; distribution unlimited.
2b. DECLASSIFICATION / DOWNGRADING SCHEDULE	
4. PERFORMING ORGANIZATION REPORT NUMBER(S) NRL Memorandum Report 6366	5. MONITORING ORGANIZATION REPORT NUMBER(S)
6a. NAME OF PERFORMING ORGANIZATION Naval Research Laboratory 6b. OFFICE SYMBOL (If applicable) Code 4430	7a. NAME OF MONITORING ORGANIZATION
6c. ADDRESS (City, State, and ZIP Code) Washington, DC 20375-5000	7b. ADDRESS (City, State, and ZIP Code)
8a. NAME OF FUNDING / SPONSORING ORGANIZATION Office of Naval Research 8b. OFFICE SYMBOL (If applicable)	9. PROCUREMENT INSTRUMENT IDENTIFICATION NUMBER
8c. ADDRESS (City, State, and ZIP Code) Arlington, VA 22217	10. SOURCE OF FUNDING NUMBERS PROGRAM ELEMENT NO. 61153N; PROJECT NO.; TASK NO. RR023-01-41; WORK UNIT ACCESSION NO. DN158-016
11 TITLE (Include Security Classification) Near Field Turbulent Wake Predictions	
12. PERSONAL AUTHOR(S) Stewart, M.B.	
13a. TYPE OF REPORT Interim 13b. TIME COVERED FROM 1/88 TO present	14. DATE OF REPORT (Year, Month, Day) 1988 November 8 15. PAGE COUNT 32
16. SUPPLEMENTARY NOTATION	

17. COSATI CODES			18. SUBJECT TERMS (Continue on reverse if necessary and identify by block number)
FIELD	GROUP	SUB-GROUP	Turbulent wake, Ship wake, Numerical partially parabolic, Finite difference, CDC

19. ABSTRACT (Continue on reverse if necessary and identify by block number)

Experimental measurements of the near-field turbulent wake of a model of a self-propelled body have shown several surprising features. Numerical models using the parabolic form of the Navier-Stokes equations have some limitation when used to model this data. Two different versions of the partially parabolic form of the equations available in the literature are examined and weaknesses for the problem of the wake of a self-propelled body are discussed. A variant is proposed which accounts for the complex initial pressure field which is integral to the down-stream prediction of these wakes. It also deals with the problems connected with using incomplete experimental data as initial conditions for this type of calculation. Comparisons are made with experimental measurements of the self-propelled model with a simulated free surface. These comparisons illustrate the features of this model.

20. DISTRIBUTION / AVAILABILITY OF ABSTRACT ☒ UNCLASSIFIED/UNLIMITED ☐ SAME AS RPT. ☐ DTIC USERS	21. ABSTRACT SECURITY CLASSIFICATION UNCLASSIFIED
22a. NAME OF RESPONSIBLE INDIVIDUAL M.B. Stewart	22b. TELEPHONE (Include Area Code) (202) 767-2858 22c. OFFICE SYMBOL Code 4430

DD FORM 1473, 84 MAR 83 APR edition may be used until exhausted. All other editions are obsolete.

SECURITY CLASSIFICATION OF THIS PAGE

CONTENTS

NEAR FIELD TURBULENT WAKE PREDICTIONS

INTRODUCTION

There are several experimental and numerical studies of the turbulent wake of a self propelled body. Schetz and Favin (1977, 1979) have computed the near-body wake using an elliptic, axisymmetric model with a one-equation turbulence model. Comparisons with wind tunnel data show good agreement with axial velocity but an underprediction of the swirl velocities. Swanson and Schetz (1975) made numerical predictions of the far wake using the parabolic axisymmetric Navier-Stokes equations with a one-equation turbulence model at locations far enough downsteam where the swirl velocities could be neglected. Swean (1987) has simulated the turbulent wake for a large range of downstream locations including axial and swirl velocities using the three-dimensional parabolic Navier-Stokes equations and two-equation turbulence model with a sophisticated Reynolds stress closure. In general, comparisons with the wind tunnel data of Mitra, Neu, and Schetz (1985, 1986) were good especially when an account was made of the axial pressure gradient in the otherwise parabolic model.

The purpose of the present study is to develop a partially parabolic model of the wake of a self propelled body. The goal is to eliminate the need for measured downstream pressure data used in Swean's 1987 study while maintaining the overall good agreement with the experimental data. The following sections contain a description of the numerical model. A description of the experiments and Swean's (1987) model are available in his report.

NUMERICAL MODEL

Simplifying Assumptions

The most common form of numerical model for the Navier-Stokes equations is elliptic. Numerically, this makes no assumptions about the importance of the various terms. It does require the storage of the dependent variables over the entire domain of interest. In the case of a turbulent wake, this includes 6 dependent variables (three fluid velocities, pressure, turbulent kinetic energy and dissipation) over a domain that is relatively limited in the transverse coordinates (perpendicular to the principle flow direction) but which may be orders of magnitude larger in the axial direction.

To overcome the problem of computer storage for the dependent variables, the parabolic assumptions are usually made whenever axial diffusion terms can be ignored and the axial velocity suffers no reversal (see Patankar and Spalding, 1972). The solution may be constructed by starting from the location of the initial conditions and marching downstream storing the values of the dependent variables at the current axial location only. The advantages of this procedure are greatly reduced computer storage and often reduced cpu time.

Manuscript approved September 22, 1988.

Frequently a situation occurs where the parabolic assumptions are valid except that the axial pressure gradient is important (see Pratap and Spalding, 1976). The procedure here is similar to the purely parabolic case except that the pressure must now be stored over the entire domain and multiple sweeps through the flow field are required to calculate the pressure field. The advantage of this procedure is again reduced computer storage requirements, hovever execution times are not improved. This procedure is referred to as the partially parabolic method and we will attempt to adapt it to model the wind tunnel data of Mitra et al. (1985, 1986) for the self-propelled body with a simulated free surface.

Governing Equations

The equations describing the partially parabolic form of the Navier-Stokes equations are shown in Table 1. The distinguishing feature of these equations are that all stress gradients in the axial direction except for pressure are neglected. For this we require that 1) there is no flow reversal in the axial direction and 2) the Reynolds number is high enough that the Reynolds and viscous stresses are significant only in the directions normal to the streamlines.

Typically, this form of the Navier-Stokes equations has been used to model interior and exterior flows for which pressure influences are transmitted from a downstream location to an upstream location. The downstream pressure disturbance, for examples, may be produced by an obstruction in a duct (confined flow) or a highly curved surface (exterior flow) and is numerically transmitted upstream through successive sweeps through the domain. In these situations the initial conditions used to start the calculation are the same as for parabolic flows i.e. three velocity components and turbulent kinetic energy and dissipation.

The sequence of steps used to calculate this type of a partially parabolic flow field is the following:

1) The three dimensional pressure field is assigned guessed values, usually zero.

2) The initial values of the u, v, and w components of velocity are advanced to the next station using the parabolic procedure. Existing values of pressure are used to evaluate the pressure gradient terms in the momentum equations. Any auxiliary equations such as turbulence or temperature are advanced at this time also.

3) The pressure correction equations are used to correct the values of pressure and velocity to satisfy continuity. The pressure correction equations are cast in three dimensional form but upstream and downstream values of the correction are assumed zero. The pressure is stored for the next axial sweep.

4) A new downstream station is selected and the momentum and continuity equations are solved as in steps 2 and 3. This procedure continues until the last downstream location is reached.

5) A new axial sweep is initiated using the initial conditions and the three dimensional pressure field calculated from the previous sweep. Steps 2 through 4 are repeated until the pressure correction or, equivalently, the mass residual becomes sufficiently small.

An important feature of the procedure is that the pressure disturbance is transmitted upstream by the calculation of the axial pressure gradient causing an axial velocity gradient and mass residual which is then eliminated by adjusting the upstream value of pressure via the pressure correction equation. This does not leave the initial pressure conditions intact. For the situation where the pressure disturbance has its source downstream from the initial plane, this presents no problem.

Unfortunately, this is not the case in the current situation. The pressure disturbance is caused by the body and propeller upstream of the computational domain. The initial pressure distribution, which must be specified, has a large influence on the flow field close to the body and propeller.

When the standard method of Pratap and Spalding (1976) is used, the solution converges relatively quickly with small mass and momentum residuals. However, the procedure has no mechanism to incorporate the effects of an initial pressure distribution in the converged solution. The result is that the initial pressure distribution is annihilated by the pressure correction equation leaving a pressure distribution which does no work on the flow field. The velocity fields tend to relax monotonically toward free stream values unlike the trends apparent in the wind tunnel measurements.

Mathematically it is unusual to find both the normal velocity and the pressure specified at a boundary as it is here. The problem becomes over-specified at that location and there are not enough degrees of freedom to satisfy both the Navier-Stokes equations and continuity exactly. The standard method of Pratap and Spalding (1976) formulates the problem with non-zero initial conditions on velocity only. The complementary formulation using the initial pressure distribution instead of the axial velocity was also computed with a similar lack of success. Instead of annihilating the initial pressure as before, it is the initial axial velocity which becomes distorted.

There is a method in the literature which naturally incorporates the Dirichlet type of boundary condition on the pressure equation at the initial plane. Where the original method calculates the elliptic pressure field in a marching procedure starting at the initial plane and marching downstream, a method similar to Chilukuri and Pletcher (1980) can be used which solves the three-dimensional pressure equation and leaves the initial pressure conditions intact. The basic assumption here is that either the initial pressure gradient is zero (which again eliminates the influence of the initial pressure) or, the initial pressure and velocity conditions satisfy the Navier-Stokes equations, the continuity equation, and the modeled form of the Reynolds stresses (which is the assumption used here). Mathematically, the difference between these two methods is that the Pratap method solves an approximate equation which is used to correct

a previous estimate of pressure where the method of Chilukuri calulates the actual elliptical pressure field based on values of the velocities using the full Navier-Stokes equations.

The goal here is to find a numerical procedure using either form of the pressure/continuity equation which compromises between satisfying the Navier-Stokes equations and continuity while incorporating both the initial axial velocity distribution and initial pressure. This compromise will only be noticable near the initial plane and will depend on the quality of the initial conditions.

Method Development

As mentioned before, the first method used was the procedure of Pratap and Spalding (1972). Because this method is unable to use initial pressure conditions the solution converges to a mathematically satisfying but physically unrealistic flow field. In order to correct this deficiency in the method, a modification was used to keep the initial pressure field intact. At the beginning of each sweep, the axial velocity field was advanced using the pressure gradient between the initial pressure plane and the first calculated pressure plane downstream. The transverse velocity fields are advanced to the next downstream station. The pressure correction equation is used to correct the transverse velocity components but not the initial pressure. At the second and all subsequent stations downstream, the velocity fields are advanced and the pressure correction equation is used to correct both the pressure and transverse velocties.

This represents a simplistic way to overcome the initial pressure field problem. Unfortunately, the solution diverges at the initial plane location. The connection between the pressure at the initial plane and the first station downstream is too weak and a discontinuity in the steamwise variation of the axial velocity and pressure fields results.

To strengthen the steamwise connections in the pressure field, several modifications were used but without much success. A three dimensional elliptic version of the pressure correction equation was solved at all axial stations including the initial plane. Here again, the initial correction was used only to correct the velocity field leaving the initial pressure condition intact. This calculation also diverged. Instead of simply forming a discontinuity in the axial velocity field as the previous attempt did, this calculation eventually became unstable again at the location of the initial plane.

At a very minor increase in core requirements over the three dimensional pressure correction algorithm, the method of Chilukuri et al. (1980) can be used. This method does not use the pressure correction equation. Instead, the discretized forms of the Navier-Stokes equations are used in the continuity equation. After some manipulation, the equations can be separated into a standard form for the full pressure equations with source terms containing the velocities from the previous sweep. Although this source term appears to be difficult to compute accurately, it actually is already available from

the previous calculations of the velocity equations. In this way, there is little increase in computational effort or memory compared to the 3-D pressure correction method. The overall structure of the program is affected because the two dimensional pressure correction equation must be retained both for the initial sweep of the entire domain to generate the initial guess of the downstream pressure field and to maintain continuity in the regions where the axial pressure gradient is ignored.

There are two potential advantages using this method. The first one, which is often found in the literature, is that the convergence rate is improved because the full Navier-Stokes equations are used to satisfy continuity rather than the approximate form of the pressure correction method. More important for the current problem is that the boundary conditions for the elliptic equation are in the form of pressure rather than a pressure correction which must be surpressed at the initial plane. The coefficients linking the pressure field to the initial pressure conditions are easily calculated. It does not, however, alter the over-specified condition at the initial plane.

In practice the faster pressure convergence rate expected of this method was apparent over most of the flow field. It did not occur at the first axial station and, in fact, the calculation slowly diverged and eventually became unstable at that location.

The last two methods which have been described involve three dimensional calculation of the pressure field and, as a result, require considerably more computer storage. The memory limitations of the LCP2 Vax 11-780 threaten to make the axial grid spacing unacceptably coarse. An examination of the parabolic calculations showed that the effect of the axial pressure gradient became negligible at about x/D = 6. Thus the program was modified so that the partially parabolic region was confined to $0 < x/D < 6$ and a parabolic calculation was used to calculate the rest of the flow field $6 < x/D < 28$. An additional advantage to this procedure is that the multiple sweeps are restricted to the reduced domain and the full domain is calculated only on the last sweep, greatly reducing cpu requirements.

Modified Flow Models

All attempts to make the flow field conform to all parts of the model within the first step downstream creates a highly distorted pressure field which, in turn, causes the axial velocity gradient to become distorted. The basic method which appears to avoid this instability is to separate the calculation of the axial pressure gradient from the transverse pressure gradient in some way. Two approaches were used and their advantages and disadvantages will be discussed.

Pressure Correction Method

There are several advantages to using the pressure correction method in modified form for this problem. The most obvious is that computer storage requirements are

small. The second is that all disturbances in this type of flow situation are propogating downstream. This eliminates one of the primary advantages of three dimensional pressure calculation methods which is that downstream pressure disturbances are felt throughout the domain in one axial sweep. The final advantage is that the equation is directly formulated to annihilate the mass residual. It uses an approximate form of the Navier-Stokes equations in the continuity equation and has the property that the calculated pressure field will satisfy the Navier-Stokes equations only in the limit of zero mass residual. The approximate nature of the initial conditions should be less important using this method.

The marching form of the pressure correction equation is used here. During each sweep, the pressure is stored at each axial downstream location but the pressure gradient in the axial velocity equation is used from the previous sweep. Notice that by using the marching version of the pressure correction equation we maintain the advantage of reduced computer storage requirements compared to full three dimensional pressure or pressure correction methods.

In this way, a purely parabolic calculation is used to provide the initial axial pressure distribution. All subsequent sweeps will use the calculated pressure gradient. The difference between this formulation and the standard pressure correction method is that the initial guess for the transverse pressure field at each axial station is advanced from the immediate upstream location. The difference between the marching scheme and the three-dimensional methods is that axial effects in the marching scheme are included in the pressure equation only through the neighboring pressure correction coefficients. The values of actual upstream and downstream pressure corrections are assumed to be zero. Only the transverse velocities are adjusted using the pressure corrections. If the axial velocity is also adjusted, the effect is the same as modifying the axial pressure gradient which effectively removes the upstream pressure conditions and the resulting pressure gradient evenutally relaxes to a version which again does no work on the axial velocities.

By advancing the upsteam transverse pressure as an initial estimate and correcting only the transverse velocities, the effect of the initial pressure conditions is transmitted downstream because each new transverse pressure field is exactly the sum of the upstream pressure plus the correction needed for the actual mass residual caused by advancing one axial location. At each axial location, only one iteration of the pressure equation is needed. Because only the transverse velocities are corrected during the sweep, the mass residual cannot be eliminated during the current sweep, rather, several sweeps are needed so that the axial velocity may respond to the new pressure field. Several implicit iterations at the same axial location would produce a slightly smaller mass residual but subsequent pressure corrections would not be accurate. The first iteration would produce a pressure and velocity correction based on the actual mass residual. Further iterations at the same location would produce pressure corrections

based on the axial part of the mass residual which cannot be immediately eliminated. A distorted pressure field would result. During the last axial sweep, however, multiple implicit iterations should be used as the pressures calculated then will not be used for the axial pressure gradient and the greatest possible reduction of the mass residual is needed to accurately predict swirl velocities.

Similarly, the mass residual could be eliminated during a single sweep by writing the pressure correction equation only for the transverse coordinates and eliminating the upstream and downstream coefficients. This forces the transverse velocities to be solely responsible for satisfying continuity. The result is that at the first station downstream of the initial condition plane the maximum swirl velocity was almost doubled and the calculated transverse pressure was no longer related to the axial variation of pressure and could not be used for this on the next sweep.

The final result of this calculation was a flow field which converged within 15 axial sweeps. Near the initial condition plane, a finite mass residual remains but downstream it quickly dies out. This finite residual appears to be caused by the approximate nature of the initial conditions. Comparisons with the experimental data will be presented in a later section.

Total Pressure Formulation

This method is actually a small modification of the method of Chilukuri (1980) and uses the same general principles as the previous method. Here, the axial sweep of the velocities and transverse pressure is exactly the same. On the first sweep, the calculation is again purely parabolic with no axial pressure gradient and the resulting three-dimensional pressure field is stored as an initial guess. On subsequent sweeps, the pressure correction equation is calculated to satisfy the transverse continuity condition in the same way as the previous method. The pressure field calculated by the pressure correction method is not stored. Instead, the three dimensional coefficients for the full pressure equation are calculated and, at the completion of each axial sweep, the full pressure field is calculated.

Here since we are not using the values of the calculated transverse pressure field for the axial pressure gradient, multiple implicit iterations at each axial location are useful to provide the best estimate of the converged, mass conserving velocity fields using the current estimate of the axial pressure variation. This will help provide the best estimates of the coefficients for the pressure equation.

This method has some of the same disadvantages of the original version which is increased computer storage over the pressure correction method. In addition, because a hybrid procedure is used, i.e. the pressure correction method is solely used for continuity and velocity correction and the total pressure method is used to calculate the axial pressure gradient, the calculation converges much more slowly requiring about 100 iterations. In addition, this method uses multiple implicit iterations on all but the

first axial sweep while the pressure correction method uses multiple iterations only during the last sweep. The final result is that the pressure correction method required approximately 1.75 hours of cpu on the LCP2 vax while the total pressure method required approximately 25 hours. How much of this difference was due to increased calculations and how much was caused by the increased need for memory paging due to the much larger memory requirements is unknown. Of course either method would require negligable cpu times on the NRL Cray.

The advantage of this method is that more of the physics of the problem are included in this calculation of the axial pressure variation because the form of the equation is nominally exact. As we shall see, the differences between the predictions of the two methods are relatively small.

COMPARISONS WITH EXPERIMENTS

The experiments used to compare with the numerical predictions have been extensively reported in Mitra, Neu, and Schetz (1985, 1986). The experiments were essentially of double axisymmetric bodies connected by a thin strut in a wind tunnel. They were used to simulate a SWATH (Small Waterplane Area Twin Hull) type ship and the plane of symmetry represents the free surface. No attempt was made to simulate the second half of this type of ship as the hulls are separated far enough in an actual ship that the merging of the wakes would not occur in the domain of interest. Several sets of experiments were run. In the situation we will be concerned with here, the free stream velocity was 45.72 m/s, both the body and its mirror image were self propelled with a 15.24 cm propeller with thrust balanced against drag using a strain guage, and transverse plane data was taken at 3.17 cm (x/D = .208), 15.24 cm. (x/D = 1), and 427 cm. (x/D = 28).

In addition, a detailed comparison between these measurements and a parabolic finite element code is reported in Swean (1987). In Swean's report comparisons were made with the mean velocities, turbulent kinetic energy, and Reynolds stresses. In order to accurately model the self-propelled body, Swean used the measured pressure profiles at the three axial positions to estimate the axial pressure gradient. In general, the agreement was very good. The purpose of the current study was to present a calculational model which would make predictions based solely on initial plane data.

Here we will compare the predictions of the present models with the experimental data and the previous parabolic predictions. Only those features of the data which are influenced by the partially parabolic features of the code will be presented. The parabolic finite element code used by Swean solved the same set of equations describing momentum transport and turbulent kinetic energy and dissipation as the present finite volume code. Continuity was satisfied in both using a Poisson type equation but the current formulation uses a predictor-corrector type formulation while the finite element code uses a penalty method. To differentiate between the two methods and a purely

parabolic (P) calculation, we will refer to Swean's method as a quasi-partially parabolic model (QPP) and the present method as modified partially parabolic (MPP).

Even though experimental data is available to initiate the calculation, this data covers only part of the domain (see Swean, 1987 for details). The data was interpolated, extrapolated,and reflected to cover the missing areas. This was made especially difficult because of the absence of true symmetry due to the rotation of the fluid caused by the propeller. This process contributes to the approximate nature of the initial conditions. Here, we use the initial conditions as formulated by Swean including the grid, the velocity fields, the turbulent kinetic energy, and the turbulent dissipation. The only modification made was to fit the data onto a staggered grid.

Comparisons between the MPP and QPP predicted and measured values of the axial minimum and maximum velocity are presented in figures 1 a and b. The most striking feature of these plots is the peak of the maximum velocity which occurs downstream of the initial plane. This peak is caused by the axial pressure gradient and shows the need for the partially parabolic assumptions. It is interesting that the predicted axial location of this peak and the location of the measured values coincides. No special effort was used in the calculation to insure this feature. A strictly parabolic calculation with no streamwise pressure gradient does not predict a downstream maximum for the axial velocity.

The QPP prediction of this data set also showed that the measured and predicted peak occured at the same axial location but this was due to the use of the measured axial pressure gradient which places the peak at that location. The value of the measured peak axial velocity is greater than the predicted value in both the QPP and MPP predictions. In the MPP calculations, the underprediction appears to be caused by the initial adjustment region directly downstream of the initial plane. During these initial calculations, mass continuity is not perfectly satisfied and some of the effect of the pressure gradient appears to be lost.

The QPP calulation requires that continuity be satisfied to within a chosen tolerance before advancing to the next axial station yet the peak value of the axial velocity is less than either the measured values or the current predictions. There are two possible explanations for this. The simplest reason is that it uses a value of the pressure gradient which is an average between the initial plane and $x/D = 1$ downstream and which has been extensively extended to cover the entire transverse plane. The other possible cause may be due to the method in which overall continuity is satisfied. For the present MPP models, during any sweep through the axial domain, the axial pressure gradient used was calculated from the previous sweep. The traditional method of satisfying continuity at each axial location is to correct all three components of velocity. It is easy to show that by correcting the axial velocity in the MPP method, the effect is to change (usually reducing) the axial pressure gradient. Assuming for the moment that the finite element QPP code is similar in this respect, the downstream

axial velocity peak would have been reduced by a strict continuity requirement at the first several stations. This could possibly explain the smaller peak found in the QPP model compared to the MPP model.

The other profile shown is the minimum axial velocity either at the body center or behind the strut at the simulated free surface. Initially this minimum occurs at the center of the body but, at some distance past the x/D=1 station, the velocity deficit behind the strut at the symmetry line becomes the minimum. The use of the axial pressure gradient in both the QPP and MPP calculations causes the velocity deficit in both locations to relax back to free stream values much more quickly than a purely parabolic prediction. In fact, the current MPP as well as the QPP calculation appears to have slightly overpredicted the relaxation rate compared to the experiments.

Qualitatively, both the QPP and MPP calculations show the same behavior. Quantitatively, the velocity defect behind the body center for the MPP method continues to relax back to the free stream value faster than the QPP method. This changes the location where the minimum axial velocity moves from the body center to the intersection of the strut and symmetry line. For the MPP method, this occurs at about x/D = 3 and for the QPP method at about x/D = 7. The experimental measurements only shows that it occurs sometime between the x/D = 1 and x/D = 28 stations.

Figures 2, 3, and 4 shows the development of the swirl velocity compared to the experimental values. In the plot of values at x/D = 1 the predictions agree well with the measured values. The maximum value of swirl is slightly less than either the measured or the QPP model. The reason for this is that this value is very sensitive to the mass continuity calculations upstream. Since continuity is not used as a criterion for the local convergence during each sweep, a set number of iterations (from 3 to 10) were performed at each axial location before advancing downstream. The swirl predictions improved as the number of iterations increased but the overall execution time quickly became excessive. The calculations using 20 iterations in the last sweep of the pressure correction form of the MPP model showed that this minor difference (seen here for 10 iterations) was due to this sensitivity.

A more interesting difference is seen in the comparison at x/D = 28. Again the value for the maximum swirl velocity calculated by the MPP method is slightly low. The center of the swirl has also moved slightly to the right unlike the QPP method. The reason for this illustrates the differences in the computational methods. The finite volume calculation uses a hybrid upwind/central difference method. The finite element method uses something similar to artificial dissipation to maintain numerical stability and the effect of this was minimized for this calculation by Swean. Thus the finite volume calculation has considerably more numerical diffusion and the effect of the mirror image body and propeller was felt more quickly. The effect of this image is an induced translation of the propeller vortex in the direction of the tangential velocity at the symmetry line similar to the self induced translation of a vortex pair (see for

example Sarpkaya, 1982). While the effect is real, it is obviously overestimated here due to the excessive numerical diffusion. A simple solution for this problem is the use of third order upwind techniques such as the QUICK scheme (Freitas et al. 1985). At this axial location some countersign vorticity begins to appear where the swirl velocities interact with the right boundary. This is again caused by the translation of the propeller vortex. The predictions are good nevertheless.

A comparison of the axial decay rate of turbulent kinetic energy at two locations for both the MPP and QPP calculations is shown in figures 5 a and b. The top line shows k for the location directly behind the body at the propeller center. At the initial plane, the body center has a relatively low level of turbulent energy surrounded by higher levels. The QPP method predicts that at the x/D = 1 axial station, the surrounding turbulent energy was expected to diffuse inward, eliminating the depression in k and raising the value above that at the initial plane. Measurements seem to indicate much less diffusion was present leaving the depressed center area intact with a value less than the initial value at x/D = 1. As shown here, the MPP predictions are that the value at the body center does drop going downsteam. This agreement with the measurements may be more fortuitous than accurate however. In figures 6 a-d the radial distribution of k at x/D = 1 is shown. Although the center value is quite reasonable, the value of the surrounding peak is depressed. The figure showing the QPP results at that location show that although the center depression is eliminated, the estimates of the surrounding peak are quite good. It appears that in the current model the generation terms in the turbulent kinetic energy equations are too crudely estimated.

The original programming was designed to produce readily recognizable code, thus the various Reynolds stress components which went into the generation terms were left intact. Derivatives of the Reynolds stresses were made using the discrete volume values which were in turn, found from the surrounding values of velocity, k and ϵ. The result is that a point value for the generation term is calculated from distant values of the other primitive variables and the smea..ig causes an underestimate. In the finite element code, all derivatives are evaluated at the point they are used with second derivatives reduced to products of first derivatives. The result is that much less diffusion is expected.

A future improvement on this code would be to reduce the source terms in the turbulence equations to primitive variables (u, v, w, k, and ϵ). This would require some fairly tedious manipulations and the coding would be much less transparent but numerical diffusion should be reduced and the peaks in turbulent kinetic energy should be higher. Whether the center depression in turbulent kinetic energy would be maintained is not clear and the numerical diffusion would still be greater than that found in the finite element calculations.

The experimental data has a second, much higher peak value of turbulent energy at about R/D = .4 as shown in figure 6. This peak actually increases by about 50% by

x/D = 1 from the initial plane. All of the models predicted approximately equivalent results for this feature. Instead of increasing, the peaks decayed by about 50%. At this location, velocity gradients and predicted turbulent production are small. It appears the the measured increase in turbulent energy is actually caused by velocity fluctuations due to the passing of the propeller tip. An analysis of the turbulent spectrum by Mitra et. al. (1986) shows a large peak at the primary and harmonic frequencies associated with propeller rotation.

Comparisons Between Current Methods

Thus far, all results shown have been for the total pressure formulation version of this model. As was described earlier, this version uses the complete Navier-Stokes eqution in the continuity equation to calculate pressure. It was used primarily because it contains more of the physics in complete form than does the method using the pressure correction. There are two reasons for preferring the pressure correction version if the accuracy is comparable. First, the execution time is reduced by a factor of 16 and, second, storage is reduced by a factor of 8. Of course, the magnitude of these reductions are specific to this problem but they appear to be conservative estimates.

Some general observations concerning the predictions produced by both versions will illustrate the differences. First, they differ primarily in the way they calculate the axial pressure distribution. The total pressure version can be expected to produce a better estimate of the axial pressure distribution at the expense of small errors in the satisfaction of continuity near the initial plane. This is because the axial pressure distribution is calculated using a global, three dimensional calculation but the equations used are different from the ones used to calculate transverse pressure to satisfy continuity. The pressure correction method is expected to satisfy the continuity equation better but produce a cruder estimate of the axial pressure gradient. This is because axial pressure is calculated using an approximate equation but the axial and transverse pressure calculations are consistant (if separate). Finally, if continuity is satisfied exactly, both methods should give equivalent results.

Figure 7 contains a comparison between the decay of the maximum swirl velocity for the total pressure version, the pressure correction version, and the measurements. The pressure correction version is better at satisfying the transverse part of the problem. At x/D = 1 the maximum swirl is equivalent to the QPP finite element code and closer to the experimental measurements. In addition, the maximum mass residual (which naturally occurs just downstream of the initial conditions) is much less for the pressure correction method than the total pressure version.

The total pressure version appears to be better at satisfying the axial part of the problem. Comparisons between the maximum and minimum axial velocity as shown in figure 8 are, in general, better using this version. In addition, mass continuity is satisfied much better using this method after a few downstream steps. This is expected

once the problems associated with the initial conditions die out. After about x/D = 5, both methods give equivalent results. This is expected since the mass residual of both quickly becomes small downstream of the initial plane.

Comparisons between predicted and measured pressure at the downstream locations show only general similarities. Figure 9 shows the variation of the minimum and maximum pressure as a function of axial position. The trends are the same but the maximum pressure difference is larger for the pressure correction method and appears to be closer to the measured values.

Figures 10 a - c shows that the calculated transverse pressure distribution had only a general resemblence to the measured distribution at x/D = 1. Figure 10a shows the interpolated experimental pressure data at x/D = 1 and figures 10 b-c show the distributions computed by each of the two methods described above. With reference to figure 10a, however, it should be noted that the experiments were principally confined to the 2nd quadrant (upper left) with the only additional data existing along the $\theta = 225°$ and 270° radials (as measured counter-clockwise from the right horizontal axis). Since the only natural plane of symmetry for the wind-tunnel configuration is z/D = 1, it was necessary to interpolate very sparse data to initialize the 3rd quadrant after which the data were reflected to quadrants 4 and 1, either symmetrically or anti-symmetrically as appropriate. As a consequence any data structure shown can be misleading especially in quadrants 3 and 4. The primary development in the calculations here is the transition of the pressure at the center of the body from a large positive pressure to the minimum value of negative pressure. Surrounding the body center is a region of high pressure. Otherwise, the experimental values show much more detailed structure. Whether or not some of this structure is the result of the extrapolation and interpolation routines used to map the data over the entire domain is unknown. Here again there are differences between the two calculation methods. The complete pressure formulation captured the tighter structure better while the pressure correction method estimated the total pressure difference better.

In figures 11 a and b, the calculated pressure distribution at x/D = 28 definitely shows the influence of the image body and the drag wake of the strut on the calculation. Interestingly, this is also clearly seen in the experimental data. At this axial location there was a strong, rectangular depression in the experimental pressures which seems to be either an artifact of the measurement technique or a pressure drop due to the wind tunnel walls and this was removed. As was described earlier, the effect of the image body was not evident in the swirl velocity data at this axial location.

CONCLUSIONS

The near field turbulent wake of a self propelled body presents several interesting challenges for numerical prediction schemes. The domain of interest is many times larger in the principle flow direction than in the transverse directions which indicates

the use of the parabolized form of the Navier-Stokes equations. At regions very close to the body, reversed flow makes these techniques invalid. At locations far enough from the body that the axial velocity is unidirectional, the flow field can be adequately described in the upstream plane only by using all velocity components, turbulent model components (such as k and ϵ), and the pressure. For most numerical schemes this represents an over-specified condition.

Two methods are shown to deal with this problem within the context of the partially parabolic equations. In both, the primary concept is to separate the calculation used for local mass continuity and streamwise pressure gradient. In both cases primary emphasis is placed on the local continuity equation and the results of that calculation is used to estimate the streamwise pressure variation.

Of the two methods, the procedure which uses an exact equation to calculate streamwise pressure variations and an approximate transverse continuity/pressure equation appears to match experimental measurements more closely. The procedure which uses the approximate pressure correction method for both streamwise pressure variation and transverse continuity converges much more rapidly, requires much less computer storage, and makes predictions reasonably close to the total pressure formulation and experiment.

Both methods resut in good quantitative agreement with the measured velocity data in the near-wake region and do so without the necessity to empose the emperical pressure data as was done in the QPP calculation.

ACKNOWLEDGEMENTS

This work was supported by the Office of Naval Research (Code 12). I would like to thank Dr. T. F. Swean Jr. for his assistance in obtaining the experimental data, initializing the turbulence model, discussions concerning the interpretation of many of the features of the data, and help making comparisons with his studies of this data.

REFERENCES

1. Chilukuri, R. And Pletcher, R. H. (1980), "Numerical Solutions to the Partially Parabolized Navier-Stokes Equations for Developing Flow in a Channel," Numerical Heat Transfer, Vol. 3, pp. 169-188.

2. Freitas, C. J., Street, R. L., Findikakis, A. N., and Koseff, J. R., (1985), "Numerical Simulation of Three-Dimensional Flow in a Cavity," Int. J. Num. Meth. Fluids, Vol. 5, pp. 561-575

3. Mitra, P.S., Neu, W.L., and Schetz, J.A., (1985), "Effect of a Free Surface on the Wake of a Slender Body," VPI-Aero-146, Virginia Polytechnic Institute and State University, Blacksburg, Va.

4. Mitra, P.S., Neu, W.L., and Schetz, J.A., (1986), "Effect of a Free Surface on the Wake of a Self-Propelled Slender Body," VPI-Aero-153, Virginia Polytechnic Institute and State University, Blacksburg, Va.

5. Patankar, S.V. and Spalding, D.B. (1972), "A Calculation Procedure for Heat, Mass, and Momentum Transfer in Three-Dimensional Parabolic Flows'" Int. J. Heat Mass Transfer, Vol. 15, p.1787.

6. Patankar, S.V. (1980), "Numerical Heat Transfer and Fluid Flow", Hemisphere, Washington D.C.

7. Pratap, V.S. and Spalding, D.B. (1976), "Fluid Flow and Heat Transfer in Three-Dimensional Duct Flows," Int. J. Heat Mass Transfer, Vol. 19, p.1183.

8. Sarpkaya, T., (1983), "Trailing Vortices in Homogeneous and Density Stratified Media," J. Fluid Mech., Vol. 136, pp. 85-109.

9. Schetz, J.A. and Favin, S., (1977), "Numerical Solution for the Near Wake of a Body with Propeller," J. of Hydronautics, Vol. 11, pp. 136-141.

10. Schetz, J.A. and Favin S., (1979), "Numerical Solution of a Body-Propeller Combination Including Swirl and Comparisons with Data," J. of Hydronautics, Vol. 13, pp 46-51.

11. Swanson, R.C. and Schetz, J.A., (1975), "Calculations of the Turbulent Wake Behind Slender Self-propelled Bodies with a Kinitic Energy Method," J. of Hydronautics, Vol. 9, pp. 78-80.

12. Swean, T.F., Jr., (1987), "Calculations of the Turbulent Wake Behind a Slender Self-Propelled Double-Body and Comparisons with Experiment," NRL Memorandum Report 6075.

Table 1 – Parabolic Form of the Governing Equations

Momentum:

$$\rho\frac{\partial(U^2)}{\partial x}+\rho\frac{\partial(VU)}{\partial y}+\rho\frac{\partial(WU)}{\partial z}=\frac{\partial\tau^t_{u,xz}}{\partial y}+\frac{\partial\tau^t_{u,xy}}{\partial z}-\frac{\partial P}{\partial x}+F_x$$

$$\rho\frac{\partial(UV)}{\partial x}+\rho\frac{\partial(V^2)}{\partial y}+\rho\frac{\partial(WV)}{\partial z}=\frac{\partial\tau^t_{v,xz}}{\partial y}+\frac{\partial\tau^t_{v,xy}}{\partial z}-\frac{\partial P}{\partial y}+F_y$$

$$\rho\frac{\partial(UW)}{\partial x}+\rho\frac{\partial(VW)}{\partial y}+\rho\frac{\partial(W^2)}{\partial z}=\frac{\partial\tau^t_{w,xz}}{\partial y}+\frac{\partial\tau^t_{w,xy}}{\partial z}-\frac{\partial P}{\partial z}+F_z$$

Continuity:

$$\frac{\partial U}{\partial x}+\frac{\partial V}{\partial y}+\frac{\partial W}{\partial z}=0$$

Turbulent Kinetic Energy:

$$\frac{\partial(Uk)}{\partial x}+\frac{\partial(Vk)}{\partial y}+\frac{\partial(Wk)}{\partial z}+\frac{\partial}{\partial y}((\frac{C_k k}{\epsilon}\overline{v'^2}-\nu)\frac{\partial k}{\partial y})+\frac{\partial}{\partial z}((\frac{C_k k}{\epsilon}\overline{w'^2}-\nu)\frac{\partial k}{\partial z})+$$

$$\frac{\partial}{\partial y}(\frac{C_k k}{\epsilon}\overline{v'w'}\frac{\partial k}{\partial z})+\frac{\partial}{\partial z}(\frac{C_k k}{\epsilon}\overline{v'w'}\frac{\partial k}{\partial y})+\overline{u'v'}\frac{\partial U}{\partial y}+\overline{u'w'}\frac{\partial U}{\partial z}+\epsilon=0$$

Turbulent Dissipation:

$$\frac{\partial(U\epsilon)}{\partial x}+\frac{\partial(V\epsilon)}{\partial y}+\frac{\partial(W\epsilon)}{\partial z}+\frac{\partial}{\partial y}(\frac{C_k k}{\epsilon}\overline{v'^2}\frac{\partial\epsilon}{\partial y})+\frac{\partial}{\partial z}(\frac{C_k k}{\epsilon}\overline{w'^2}\frac{\partial\epsilon}{\partial z})+$$

$$\frac{\partial}{\partial y}(\frac{C_\epsilon k}{\epsilon}\overline{v'w'}\frac{\partial\epsilon}{\partial z})+\frac{\partial}{\partial z}(\frac{C_\epsilon k}{\epsilon}\overline{v'w'}\frac{\partial\epsilon}{\partial y})+\frac{\epsilon}{k}C^1_\epsilon\overline{u'v'}\frac{\partial U}{\partial y}+\frac{\epsilon}{k}C^1_\epsilon\overline{u'w'}\frac{\partial U}{\partial z}+C^2_\epsilon\frac{\epsilon^2}{k}=0$$

Where:

τ^t is the total Reynolds and molecular stress,e.g. $\tau^t_{u,xz}\equiv\mu\frac{\partial U}{\partial y}-\rho\overline{u'v'}$
$\frac{\partial P}{\partial x}$ is calculated according to which method is used.
P(y,z) is adjusted to satisfy continuity
u,x act in the axial or streamwise direction
v,y act in the horizontal, transverse coordinate direction
w,z act in the vertical, transverse coordinate direction
F is the momentum source term
$\{C_k, C_\epsilon, C^1_\epsilon, C^2_\epsilon\}=\{.12,.09,1.44,1.92\}$

Table 1 (cont.)

Reynolds Stresses:

$$\overline{u'^2} = C_1 k - C_2 C_4 \frac{k^3}{\epsilon^2}((\frac{\partial U}{\partial y})^2 + (\frac{\partial U}{\partial z})^2) - 2C_4 \frac{k^2}{\epsilon}(\frac{\partial U}{\partial x})$$

$$\overline{v'^2} = C_3 k - C_2 C_4 \frac{k^3}{\epsilon^2}(\frac{\partial U}{\partial y})^2 - 2C_4 \frac{k^2}{\epsilon}(\frac{\partial V}{\partial y})$$

$$\overline{w'^2} = C_3 k - C_2 C_4 \frac{k^3}{\epsilon^2}(\frac{\partial U}{\partial z})^2 - 2C_4 \frac{k^2}{\epsilon}(\frac{\partial W}{\partial z})$$

$$\overline{u'v'} = -C_4 \frac{k^2}{\epsilon}\frac{\partial U}{\partial y} - C_2 C_4 \frac{k^3}{\epsilon^2}(\frac{\partial U}{\partial z}(\frac{\partial V}{\partial z} + \frac{\partial W}{\partial y}) + 2\frac{\partial U}{\partial y}(\frac{\partial U}{\partial x} + \frac{\partial V}{\partial y}))$$

$$\overline{u'w'} = -C_4 \frac{k^2}{\epsilon}\frac{\partial U}{\partial z} - C_2 C_4 \frac{k^3}{\epsilon^2}(\frac{\partial U}{\partial y}(\frac{\partial W}{\partial y} + \frac{\partial V}{\partial z}) + 2\frac{\partial U}{\partial z}(\frac{\partial U}{\partial x} + \frac{\partial W}{\partial z}))$$

$$\overline{w'v'} = -C_4 \frac{k^2}{\epsilon}(\frac{\partial V}{\partial z} + \frac{\partial W}{\partial y}) - C_2 C_4 \frac{k^3}{\epsilon^2}(\frac{\partial U}{\partial z}\frac{\partial U}{\partial y})$$

$$\{C_1, C_2, C_3, C_4\} = \{.94, .067, .56, .068\}$$

Pressure Equations:

Total Pressure Formulation:

$$A_p P_p = \sum_1^6 \rho D_i' P_i A_i + (\rho \widehat{U}_u - \rho \widehat{U}_d)\Delta y \Delta z + (\rho \widehat{V}_e - \rho \widehat{V}_w)\Delta x \Delta z + (\rho \widehat{W}_n - \rho \widehat{W}_s)\Delta x \Delta y$$

where
$\widehat{U}_i$ are the reduced velocity components
$\widehat{U}_i = \frac{1}{A_p{}^u}[\sum_1^4 A_i{}^u + B^u + D_{p,u}{}^u]$
$\widehat{V}_i = \frac{1}{A_p{}^v}[\sum_1^4 A_i{}^v + B^v + D_{p,v}{}^v]$
$\widehat{W}_i = \frac{1}{A_p{}^w}[\sum_1^4 A_i{}^w + B^w + D_{p,w}{}^w]$
P_i are the pressures at location i
A_i, B_i, D_i, are coefficients from the momentum equations

Pressure Correction Formulation:

$$A_p P_p' = \sum_1^6 \rho D_i' P_i' A_i + (\rho U_u - \rho U_d)\Delta y \Delta z + (\rho V_e - \rho V_w)\Delta x \Delta z + (\rho W_n - \rho W_s)\Delta x \Delta y$$

where
U_i are the calculated velocities at the control volume faces before continuity correction.
P_i' are the pressure corrections at location i

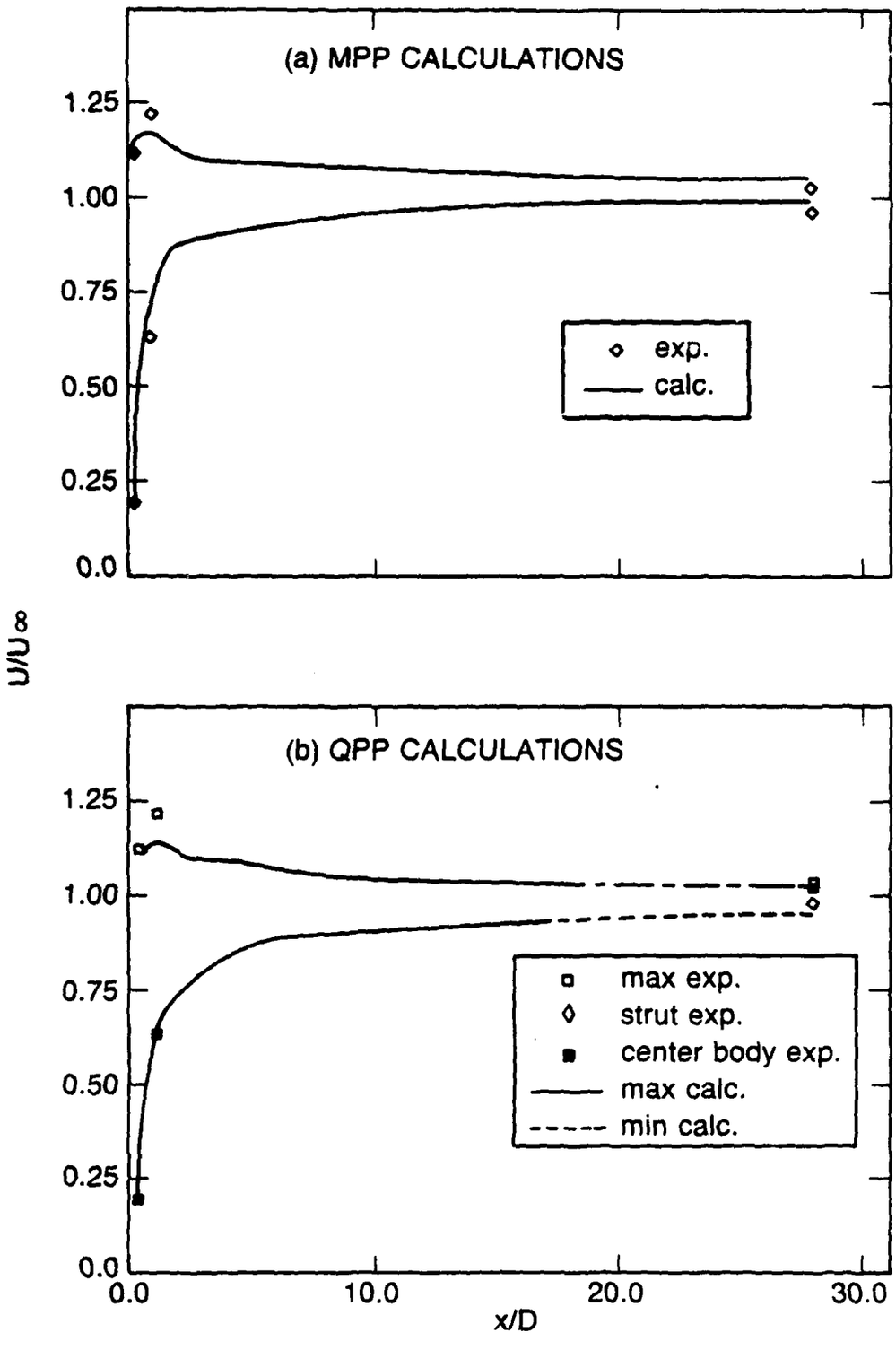

Fig. 1 - Axial Distributions of Minimum and Maximum Streamwise Velocity

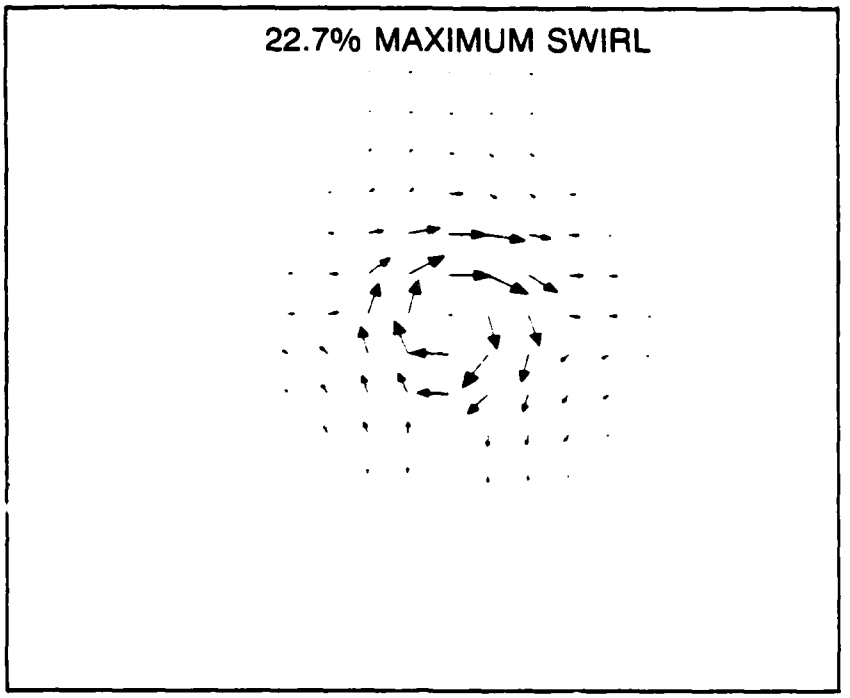

Fig. 2 - Initial Plane Swirl Vectors at x/D=.208

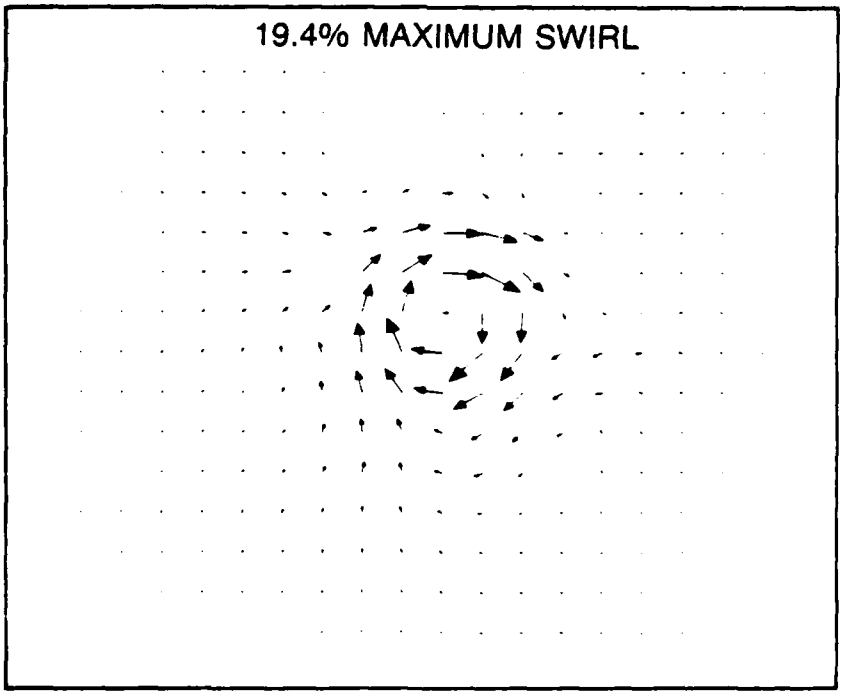

Fig. 3 - Swirl Vectors at x/D=1

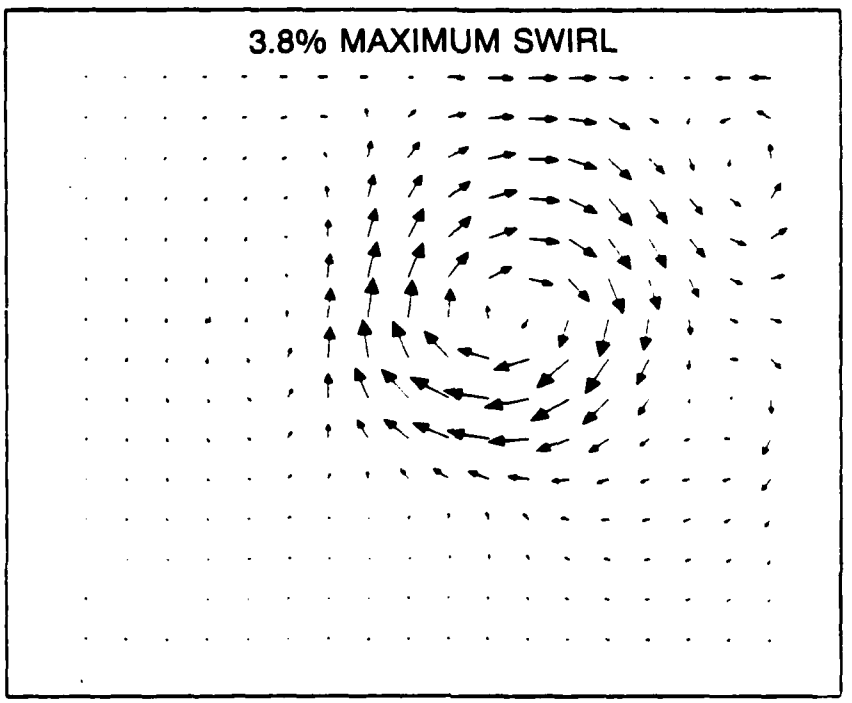

Fig. 4 - Swirl Vectors at x/D-28

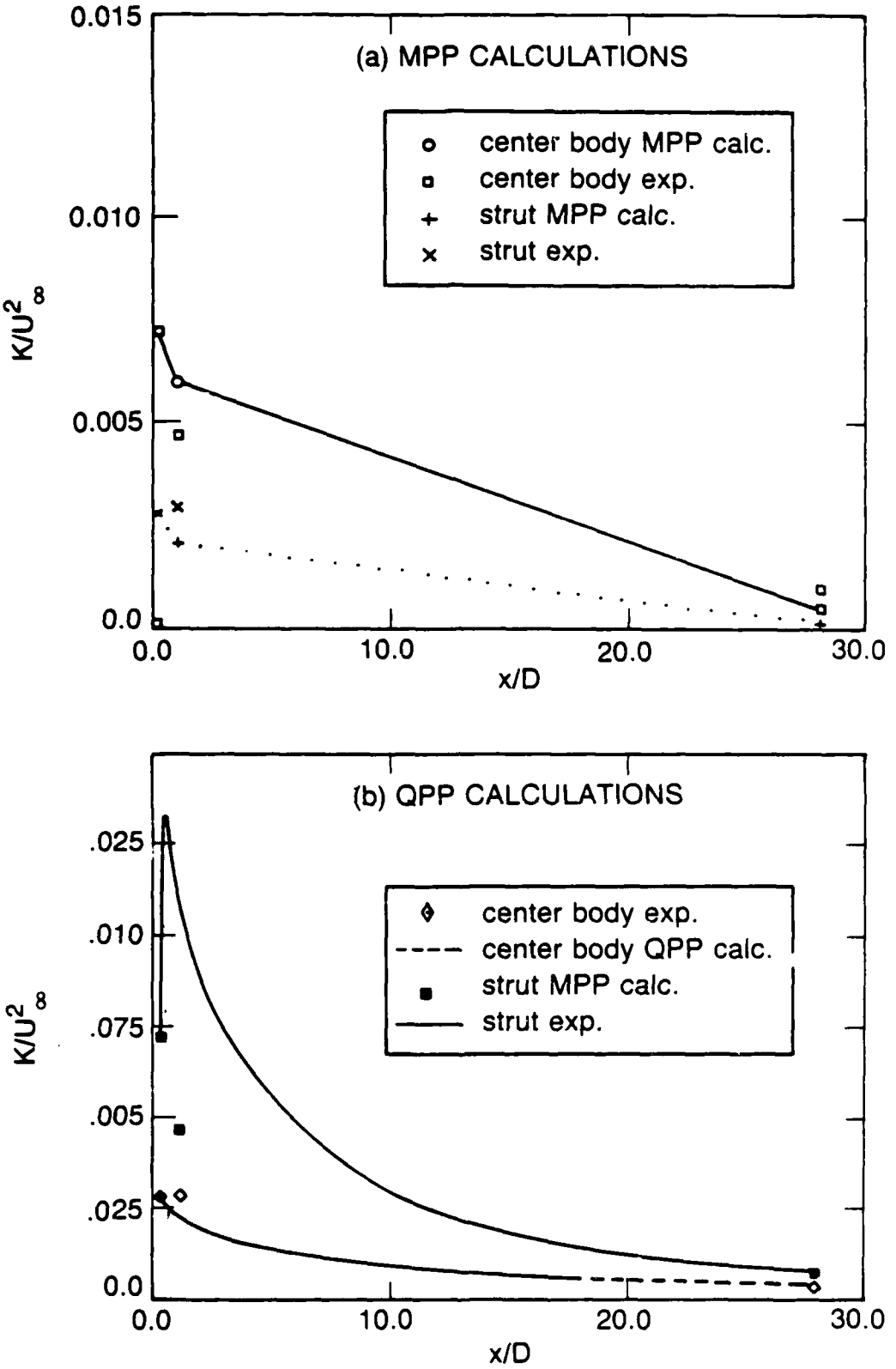

Fig. 5 - Axial Decay of Turbulent Kinetic Energy

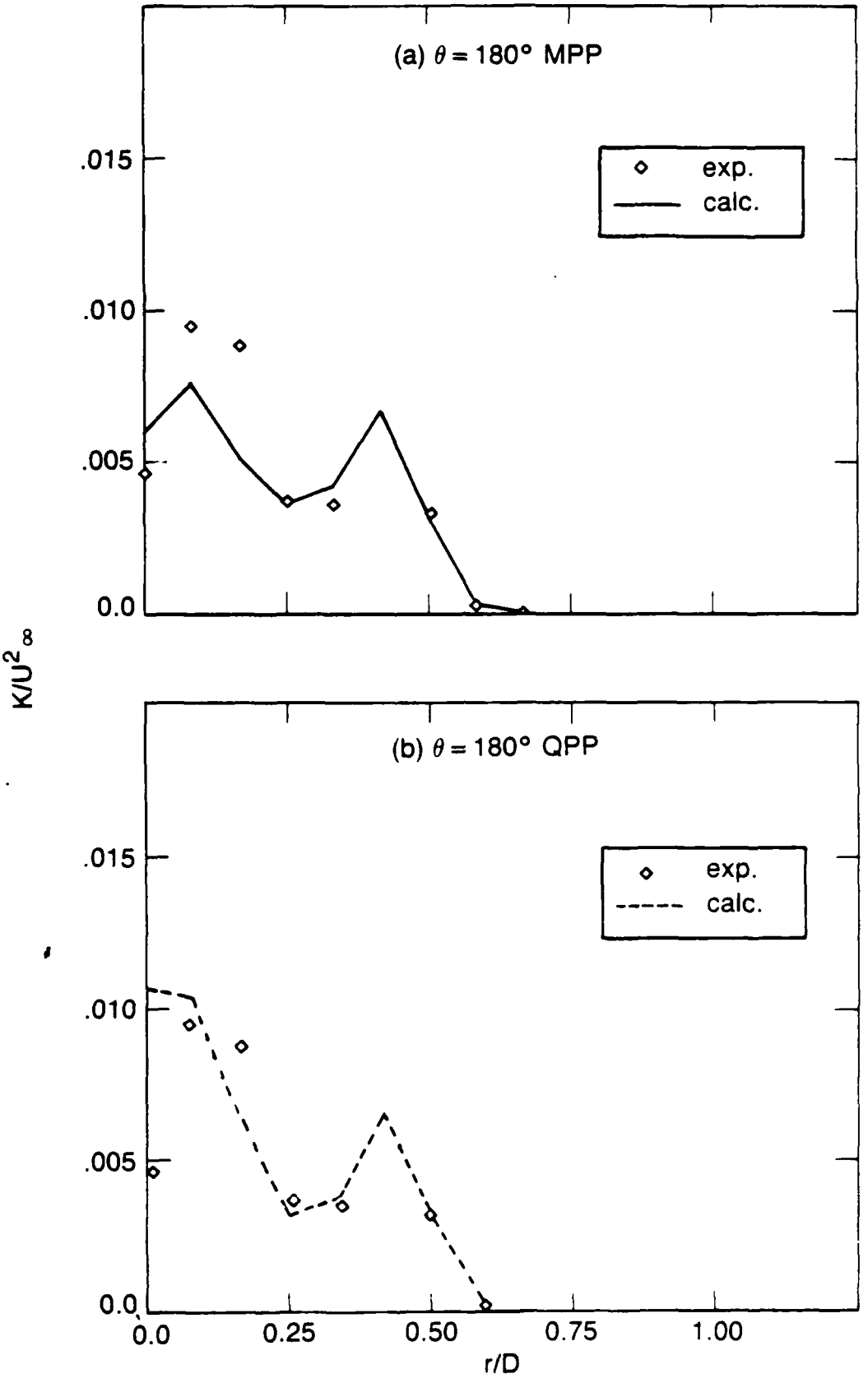

Fig. 6 - Radial Distribution of Turbulent Kinetic Energy x/D = 1

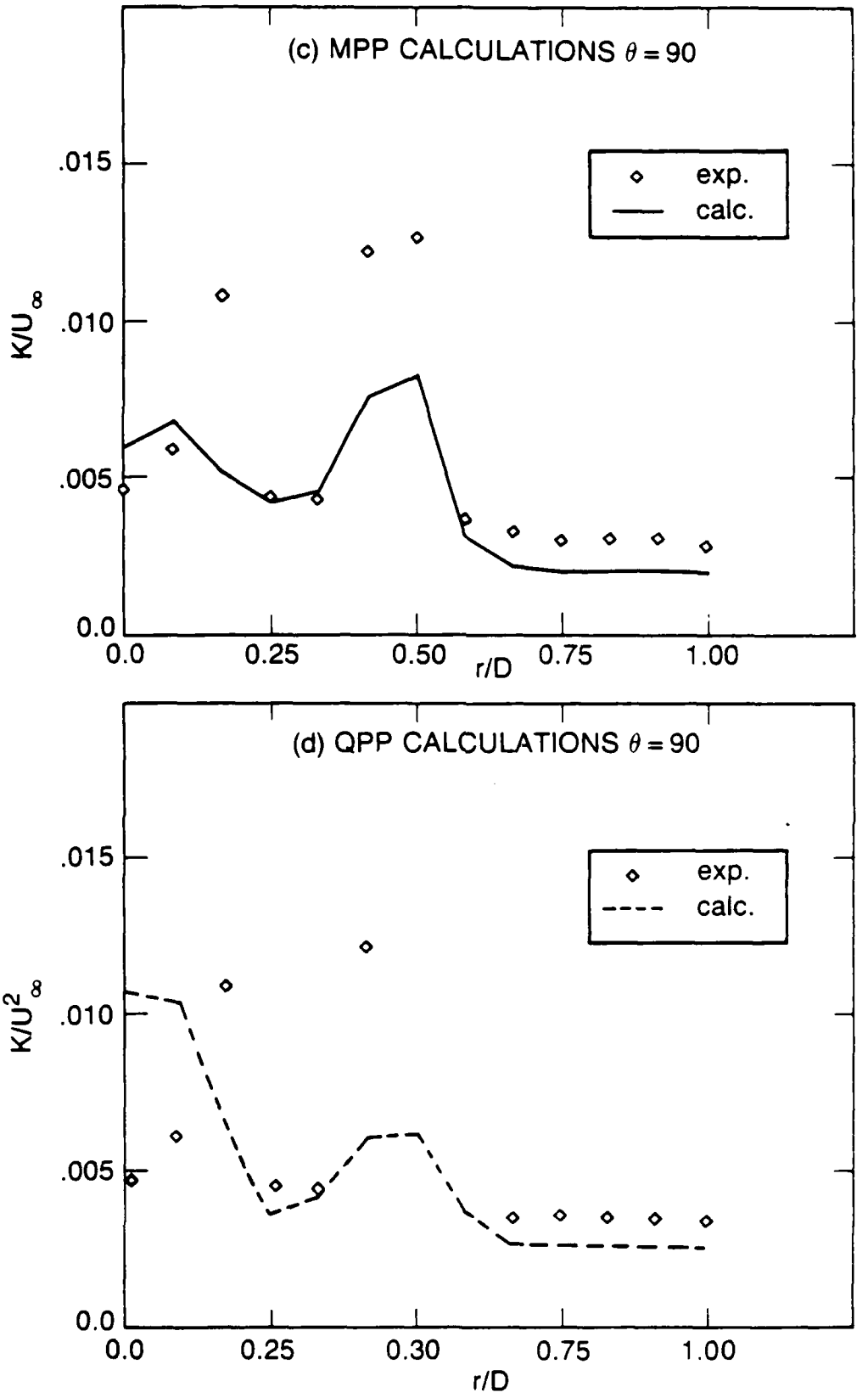

Fig. 6 - Radial Distribution of Turbulent Kinetic Energy

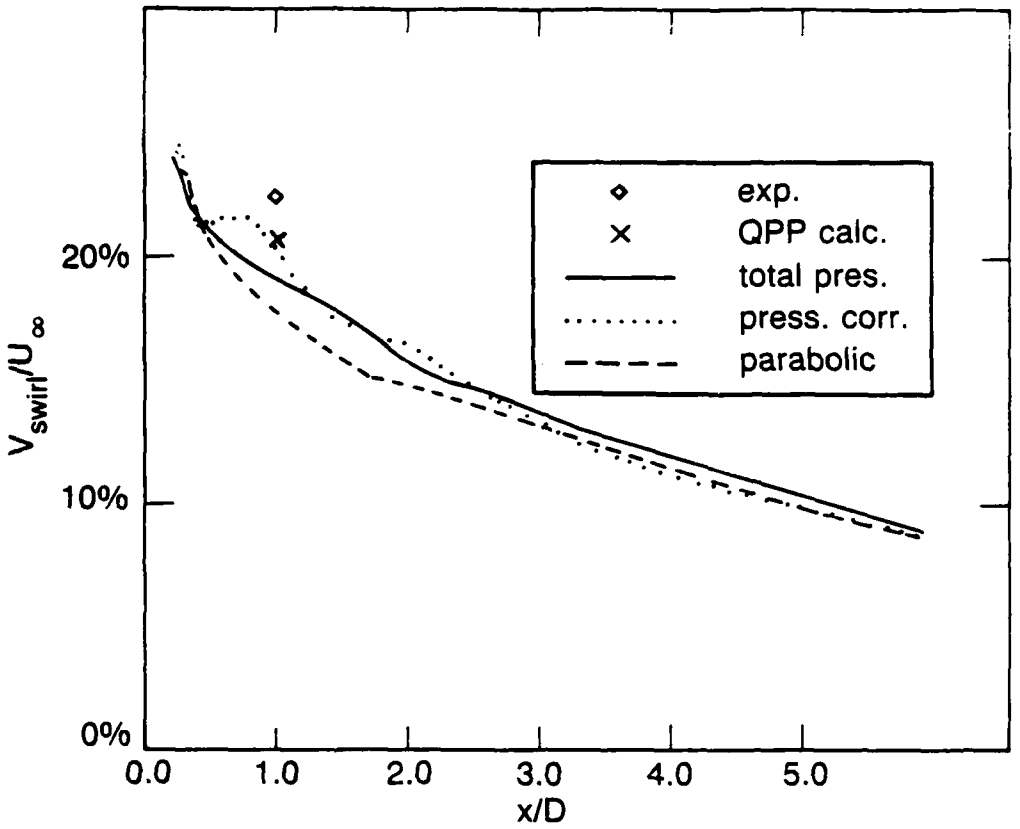

Fig. 7 - Axial Decay of the Maximum Swirl Velocity

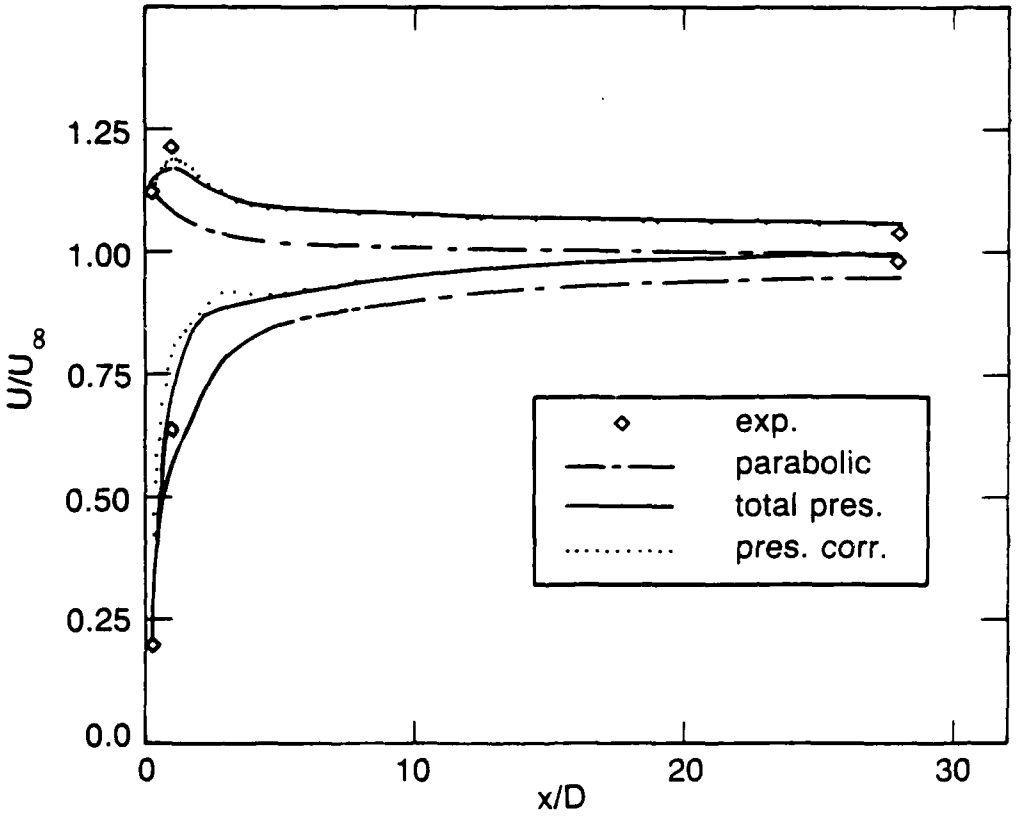

Fig. 8 - Comparison of Minimum and Maximum Axial Velocities

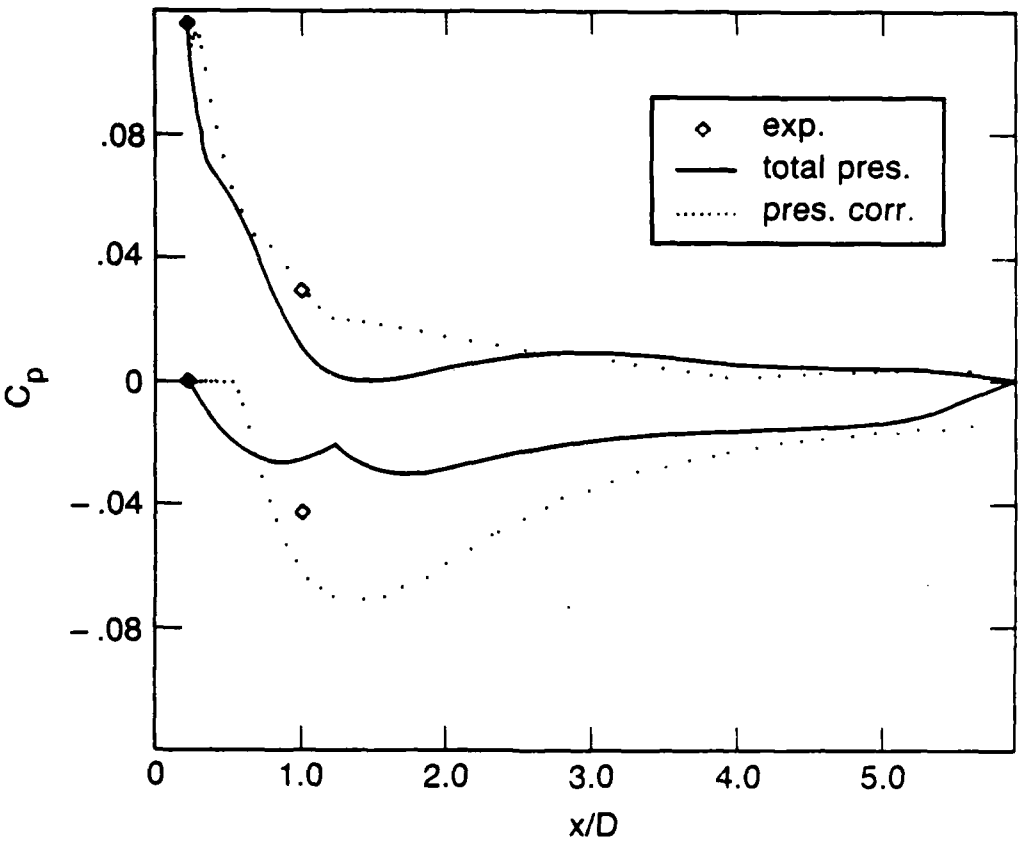

Fig. 9 - Axial Distribution of Minimum and Maximum Pressure

(a) EXPERIMENTAL

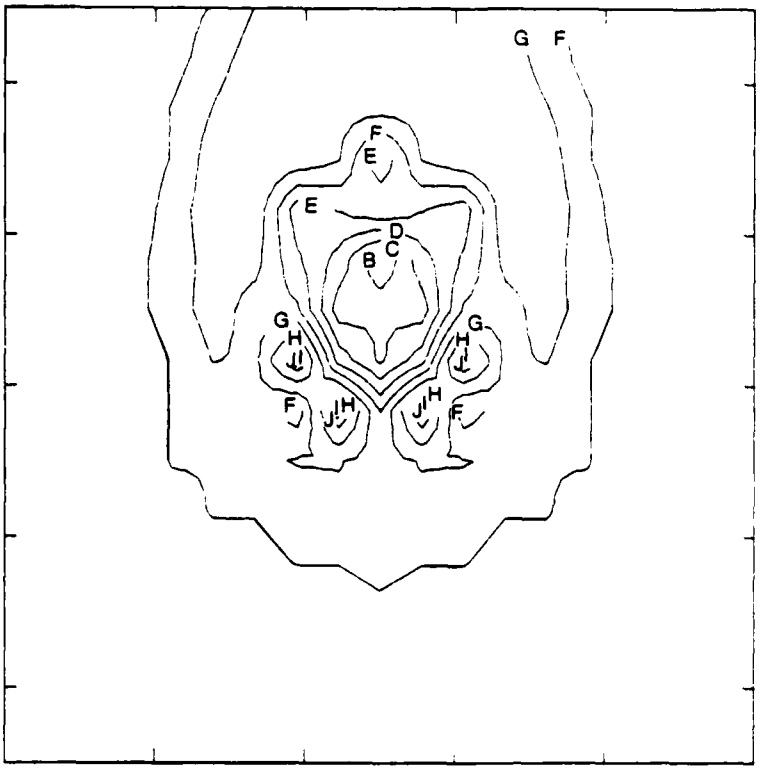

C_p

A = – .041
B = – .031
C = – .021
D = – .011
E = – .001
F = .009
G = .019
H = .030
I = .040
J = .050

(b) TOTAL PRESSURE CALCULATION

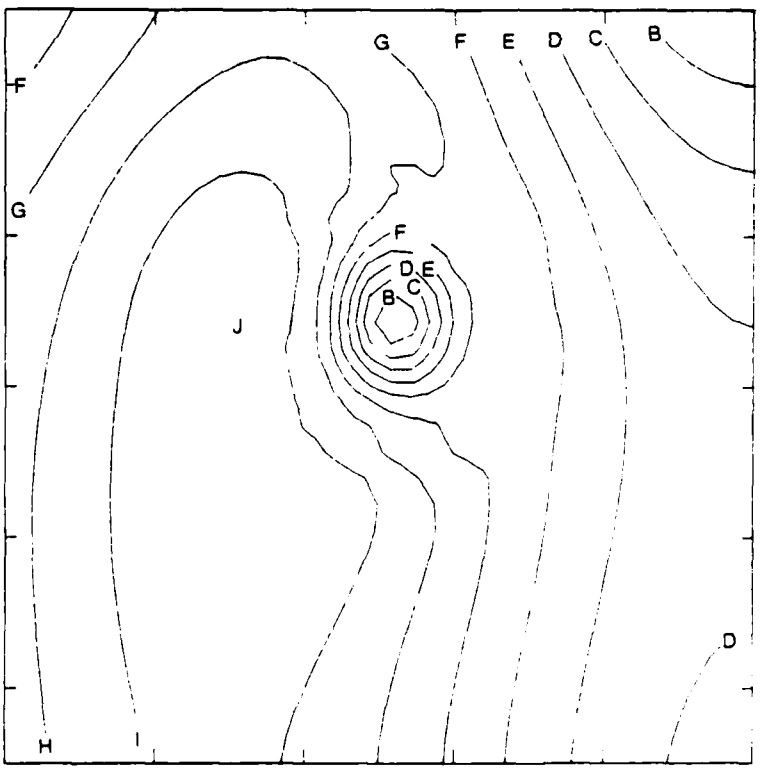

C_p

A = – .014
B = – .009
C = – .004
D = .001
E = .007
F = .012
G = .017
H = .023
I = .028
J = .033

Fig. 10 - Transverse Pressure Distribution at x/D = 1

(c) PRESSURE CORRECTION CALCULATION

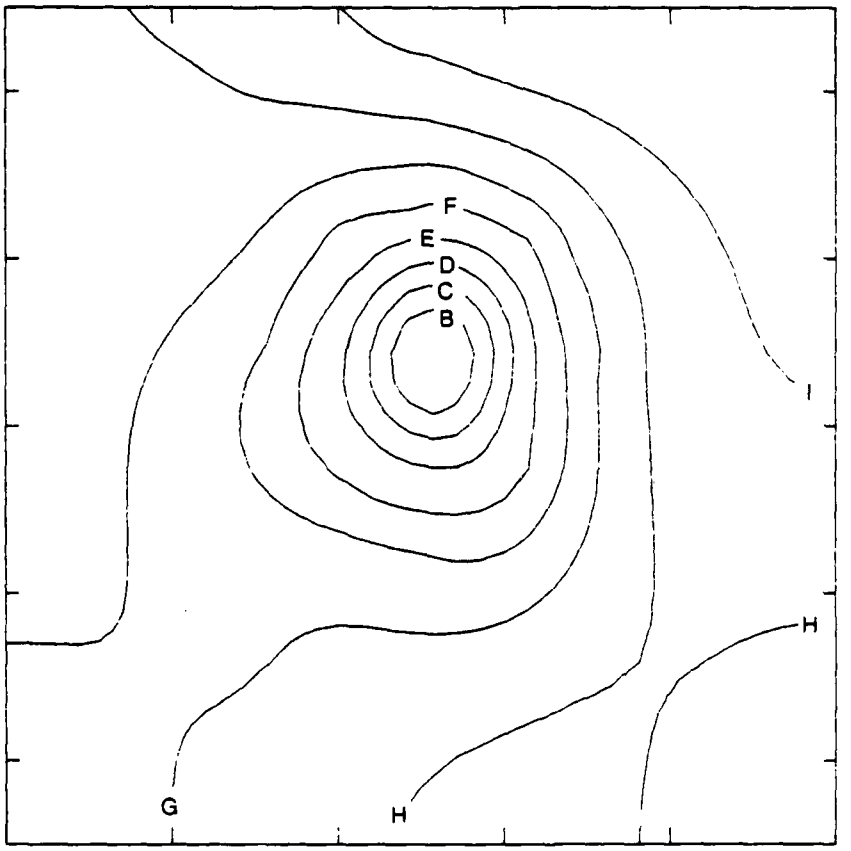

C_p

A = – .063
B = – .053
C = – .043
D = – .033
E = – .023
F = – .013
G = – .003
H = .007
I = .018
J = .028

Fig. 10. - Transverse Pressure Distribution at x/D = 1 (cont.)

(a) EXPERIMENTAL

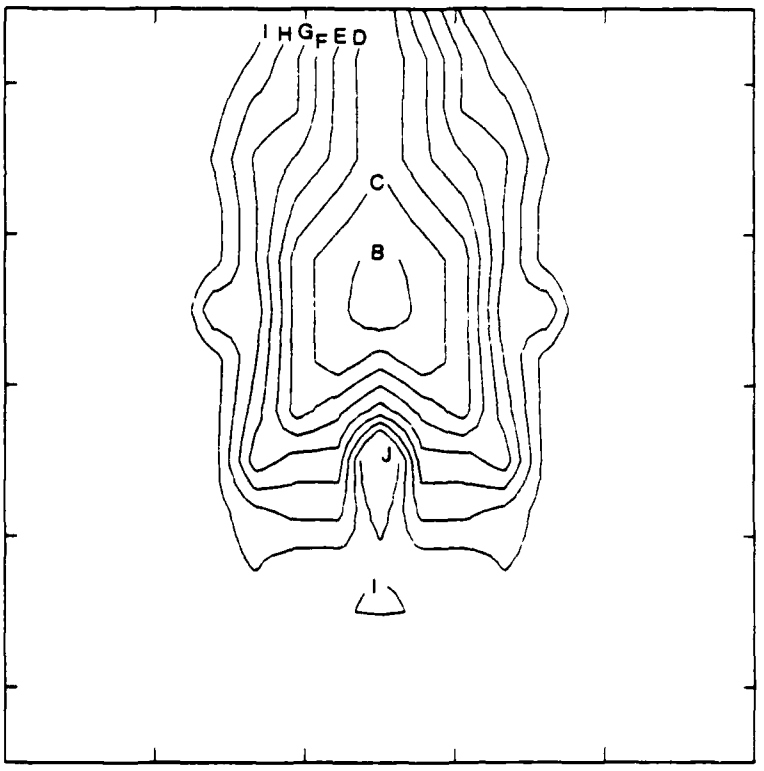

C_p

A = – .006
B = – .005
C = – .005
D = – .004
E = – .003
F = – .003
G = – .002
H = – .001
I = – .001
J = 0.0

(b) CALCULATED

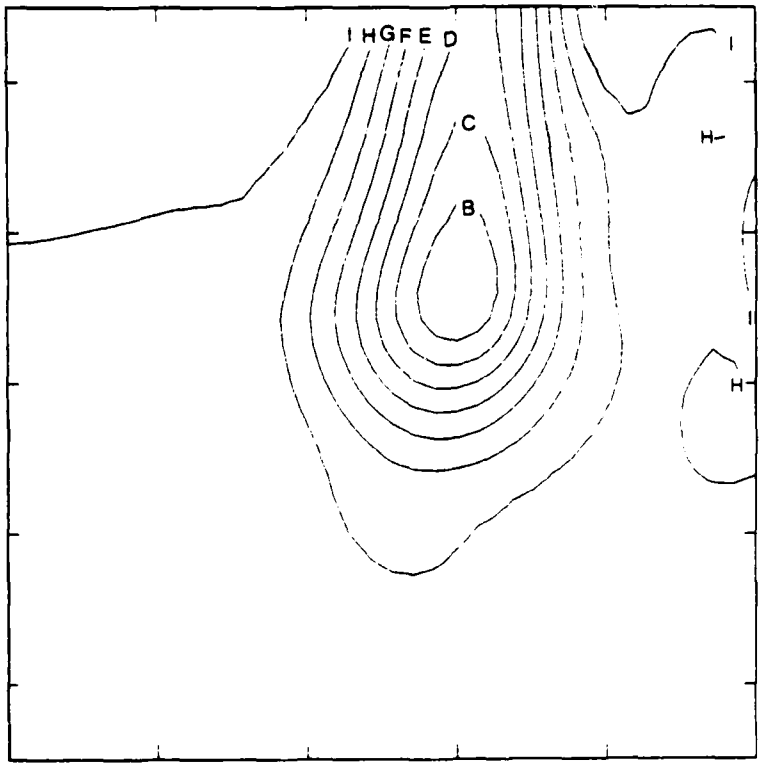

C_p

A = – .002
B = – .002
C = – .002
D = – .001
E = – .001
F = – .001
G = – .000
H = – .000
I = – .000
J = 0.0

Fig. 11 - Transverse Pressure Distribution at x/D = 28